WITHDRAWN:
The Catalytic Pyrolysis Mechanism of Cellulose On ZSM-5: Based On Py-GC/MS And Density Functional Theory

Xiaoxue Cheng
Jiangsu University
Ding Jiang
Jiangsu University
Zhen Xia
Jiangsu University
Bahram Barati
Jiangsu University
Karthickeyan Viswanathan
National Cheng Kung University
Yamin Hu
Jiangsu University
Lili Qian
Jiangsu University
Zhixia He
Jiangsu University
Shuang Wang
463475369@qq.com
Jiangsu University https://orcid.org/0000-0003-0144-1484
Hongping Li
Jiangsu Provincial Institute of Traditional Chinese Medicine: Jiangsu Province Academy of Traditional Chinese Medicine

Research Article

Keywords: cellulose, ZSM-5, catalytic pyrolysis, mechanism, density functional theory

Posted Date: May 19th, 2021

DOI: https://doi.org/10.21203/rs.3.rs-452161/v1

EDITORIAL NOTE:

The full text of this preprint has been withdrawn by the authors while they make corrections to the work. Therefore, the authors do not wish this work to be cited as a reference. Questions should be directed to the corresponding author.

Abstract

Cellulose is one of the main components of terrestrial biomass. In this study, a zeolite catalyst (ZSM-5) was used to catalyze the pyrolysis of cellulose. The components produced during pyrolysis were tested by Py-GC/MS, and the pyrolysis mechanism was analyzed by density functional theory (DFT). The results showed that furans and sugars were the primary pyrolysis products. After catalytic pyrolysis, the furfural content was significantly lower than that of non-catalytic pyrolysis. However, the yield of aromatic hydrocarbons increased significantly, especially benzene, which increased from almost zero to 13.04%. DFT further explored the specific reaction pathway of catalytic pyrolysis. It was found that under the catalysis of ZSM-5, the catalyst directly participated in most cellulose pyrolysis reactions. Also, the electrophilicity of acid sites in the reaction system played an important role. Therefore, the catalysis of the molecular sieve can significantly reduce the energy barrier of each path. In generating aromatic hydrocarbons, the decarbonylation reaction and dehydration reaction of furfural can be completely catalyzed, thereby increasing the reaction rate of generating aromatic hydrocarbons. Some deoxygenation steps occurred during the reaction, which made the catalytic pyrolysis reaction easier to develop, and improved the bio-oil quality.

Introduction

In order to achieve national energy security and energy self-sufficiency, countries are seeking new energy sources to replace petroleum-based energy Wang et al. 2017 . As a promising renewable energy source, biomass has attracted widespread attention all over the world. It can be converted into chemical substances and fuels, significantly eliminate the negative impact of fossil energy consumptions on the environment, and effectively promote carbon neutrality Alvarez et al. 2014 Anastasakis et al. 2011 Wang et al. 2016 . Cellulose is the simplest linear chain polysaccharide among the three main components of lignocellulosic biomass, consisting of several basic glucose units connected by β-1,4-glycosidic bonds Zeng and Pan 2020 Hu et al. 2020 . In the past few decades, many different technologies (biological and chemical) have been developed to convert biomass into fuel or chemical substances Sharma et al. 2015 Shen et al. 2015 . Among them, pyrolysis is a relatively mature technical method with huge advantages Jiang et al. 2020 Wang et al. 2013 Xu et al. 2020 Yuan et al. 2020 . Pyrolysis can decompose biomass into liquid, solid, and gaseous products at 400-650°C without oxygen requirement Banerjee and Mushrif 2017 . It has been widely regarded as a promising technology for converting biomass into fuel or chemicals Moazeni et al. 2019 Rathnayake et al. 2018 .

Biomass pyrolysis mainly uses wood chips or agricultural residues as raw materials Wang et al. 2017 Zeng et al. 2020 . Understanding the reaction mechanism of biomass pyrolysis will be helpful for process optimization and reactor design for industrial-scale biorefineries. However, the multi-scale complexity of biomass structures and reactions involved in pyrolysis makes the elucidation of the mechanisms challenging Wang et al. 2017 . Most of the mechanism studies of the actual biomass pyrolysis process aim to obtain the relevant kinetic parameters based on the macro-thermal decomposition process; or study the distribution of pyrolysis products of different types of biomass Torri et al. 2016 Ding et al.

2017 . However, due to its complexity, the actual biomass is still difficult to obtain more details of its specific reaction process. Exploring the reaction process of the main components of the biomass is an effective and necessary step to reveal the primary pyrolysis mechanism. In recent years, pyrolysis has been used to produce charcoal as a solid fuel, and now it has become a platform for obtaining bio-oil. Considering that bio-oil is composed of many low-content valuable chemical substances, attaining a higher yield of specific species becomes the key Moazeni et al. 2019 Fan et al. 2019 . In recent years, the selective production of value-added chemicals (sugars, phenols, furans, hydrocarbons, nitrogen-containing compounds, etc.) through the biomass's catalytic pyrolysis has become a novel and critical approach in the thermochemical conversion of biomass Dai et al. 2020 .

To use biomass reasonably, cleanly, and efficiently, catalytic pyrolysis technology has become an essential means to improve pyrolyzed bio-oil quality. Compared with traditional pyrolysis methods, catalytic pyrolysis has high efficiency, good stability, and can control the pyrolysis products Wang et al. 2017 Chen et al. 2017 . The most common practice is to add a catalyst during the pyrolysis process to selectively control the distribution of pyrolysis products and further increase the yield of the desired target product, thereby improving the bio-oil quality. Many researchers worldwide have continuously confirmed through applications that adding the molecular sieve catalysts in the cracking process can effectively improve the quality of bio-oil Zhang et al. 2018 Li et al. 2020 . Thangalazhy-Gopakumar et al. used ZSM-5 to catalyze pyrolysis of green algae to produce bio-oil, which increased the content of aromatics in bio-oil from 0.9% to 25.8% Thangalazhy-Gopakumar et al. 2012 . Lee et al. studied that the catalytic pyrolysis of microporous molecular sieve catalyst, HZSM-5, to produce high-quality bio-oil. It was observed that the contents of the oxygen-containing substances, 1, 5-dehydromannitol and 1, 4-dehydrogalactosol decreased obviously, while the contents of furan and cyclopentanone increased. The catalytic activity of HZSM-5 significantly promotes the generation of high value-added aromatic hydrocarbons Lee et al. 2014 . Rhaman et al. studied the production of aromatics by catalytic pyrolysis of pine wood by Py-GC/MS. The authors found that as the amount of ZSM-5 catalyst increased, the aromatics yield increased Rahman et al. 2020 . Nishu et al. reviewed the impact of ZSM-5 on the catalytic pyrolysis of biomass for bio-oil production. They suggested that the ZSM-5 catalyst could produce high-quality bio-oils rich in aliphatic and aromatic hydrocarbons and low oxygen content Nishu et al. 2020 . Therefore, the molecular sieve catalyst has a noticeable catalytic effect on the pyrolysis of biomass. To date, only a few articles have studied the internal mechanisms of the catalyst in depth.

Previous studies on cellulose pyrolysis were mainly carried out on thermogravimetric analyzers, which can be used in conjunction with Fourier Transform Infrared Spectroscopy (TG-FTIR) to study the weight loss of cellulose and the evolution of distinct functional groups Wu et al. 2013 Yang et al. 2018 . The analytical pyrolysis instrument combined with gas chromatography/mass spectrometer (Py-GC/MS) can directly study the products of in-situ pyrolysis Wu et al. 2013 Lu et al. 2018 Chen et al. 2019 . Researchers generally use macroscopic experimental methods to analyze the pyrolysis mechanism of cellulose Dai et al. 2018 , and some studies focus on the effect of catalysts on pyrolysis products Yang et al. 2019 . However, previous studies have only focused on the experimental phenomena caused by these catalysts. Only a few reports are available on how these molecular sieve catalysts change cellulose

pyrolysis products' selectivity. Density functional theory provides a suitable tool for exploring the mechanisms of cellulose pyrolysis from a microscopic perspective from the perspective of quantum mechanics, in which the calculated results are widely accepted in the field Shen et al. 2014 Alves et al. 2017 Shen et al. 2013 . Many reports have explained the detailed mechanisms of cellulose pyrolysis, including the formation of Levoglucosan (LG), Glycolaldehyde (HAA), furan, and other gas products under non-catalyst conditions by this method Lin et al. 2009 Zhang et al. 2015 2011 Zhang et al. 2015 Lu et al. 2016 . However, the role of ZSM-5 catalyst in the pyrolysis process at the molecular level is still not well studied.

This research aims to understand the role of the catalyst and reveal the mechanisms of the pyrolysis of cellulose catalysized by ZSM-5 Wang et al. 2013 Cao et al. 2021 . In order to thoroughly investigate the distribution of the product and further analyze the product and chemical structure, in this paper, non-catalytic fast pyrolysis of cellulose and fast catalytic pyrolysis of cellulose (ZSM-5 catalyst) were carried out on Py-GC/MS. Besides, according to the product distribution, the formation mechanisms of the leading products of cellulose catalytic pyrolysis (such as 5-hydroxymethyl furfural and levoglucan, etc.) are proposed. The M06-2X method was used to verify and analyze the catalytic reaction path at the calculation level of 6-31G(d). Ultimately, the mechanisms of the rapid pyrolysis of cellulose catalyzed by the ZSM-5 catalyst are revealed by combining experimental research and simulation analysis, which provides references and ideas for future cellulose catalytic development pyrolysis technology.

Materials And Methods

Experimental materials and instruments

Microcrystalline cellulose Avicel PH105 was purchased from Food Machinery and Chemical Corporation (FMC), which is mainly extracted from fiber-rich plants. Chemical Data Systems (CDS) Pyroprobe 5200 was used to connect with GC/MS (Trace DSQII), and Py-GC/MS system was used to separate and identify pyrolysis volatiles, and also display the distribution of products. In this experiment, ZSM-5 (SiO_2/Al_2O=3:36), a molecular sieve, was used as the catalyst, which was provided by Nankai University Catalyst Factory. The ZSM-5 molecular sieve catalyst was added to cellulose for catalytic pyrolysis test at the pyrolysis temperature of 823 °K, carrier gas flow rate of 0.2 L/min, and mass ratio of 10:1 (raw material: catalyst).

Computational models and methods

It is very imperative to select suitable model compounds through DFT research. As β-D-glucopyranose is the basic unit of cellulose polysaccharide, it can be used as a model compound to study the catalytic pyrolysis of cellulose Liu et al. 2011).

The catalyst's chemical reaction is relatively complicated, and traditional experimental methods cannot explain how the catalyst works in the pyrolysis reaction, while the DFT method can elucidate the specific reaction process. However, to study these extremely complex catalytic processes, appropriate

simplifications need to be carried out in accordance with the characteristics of the raw materials. The ZSM-5 molecular sieve catalyst selected in this work is a tetrahedral model based on SiO_4. Adjacent tetrahedrons are connected to each other by oxygen atoms sharing vertices, thereby forming a three-dimensional crystal structure. When the +4 valence Si is replaced with the +3 valence Al, the Al atom's molecular sieve framework is negatively charged. A positively charged proton (H^+) must be introduced to maintain the electrical neutrality of the system. The cluster model's size in this study was represented by 3T, which contains three SiO_4 tetrahedra (**Fig1**). Since the Si-O bond needs to be cut when constructing the cluster model, dangling bonds are generated on the boundary, and hydrogen atoms were used for saturation. The molecular structure of D-glucose is shown in (**Fig2b**). Each hydroxyl group on the sugar ring is numbered counterclockwise according to its relative position to ring O. The small cluster model (**Fig2b**) has a simple structure, fast calculation speed, and high accuracy and is often used in molecular sieves simulations Chen et al. 2019 Dumrongsakda and Ruangpornvisuti 2012 Reina et al. 2017 . The model will help study other catalysts' influence and explore new catalysts through future simulation calculations.

This research uses DFT based on quantum mechanics. The equilibrium geometry of reactants, intermediates, transition states, and products was optimized on the M06-2X/6-31G(d) calculation level using the DFT method Wang et al. 2017 . The standard thermodynamic change was obtained from the difference between the thermodynamic values of the reactants and products. According to the analysis of the vibration frequency of the reactants, intermediates, transition states, and products, all transition states have only one imaginary frequency. In contrast, the reactants, intermediates and products have no imaginary frequency Shen et al. 2013 . In addition, corresponding to the experimental conditions, the simulated temperature was set to 823 K, a typical working condition for cellulose pyrolysis. All calculations were performed on the Gaussian 16 program suite Frisch et al. 2016).

Results And Discussion

Py-GC/MS catalytic pyrolysis analysis of cellulose at 823 K

Table **1** lists the typical products of Py-GC/MS cellulose pyrolysis under the activity of ZSM-5. The catalytic pyrolysis products of cellulose on the catalyst ZSM-5 can be divided into the following compounds: furans, aromatic hydrocarbons, nitrogen-containing substances, and aldehydes, ketones, acids, hydrocarbons and small molecules. The results of Py-GC/MS catalytic pyrolysis of cellulose catalyzed by ZSM-5 indicate that the bio-oil mainly contains acids, benzenes, and furans. Where 4-methoxy-2-methylbutyl cyclopropane carboxylic acid, benzene, furfural, and levoglucan were the main products by the peak area percentages of 13.39%, 13.05%, 12.81%, and 11.24%, respectively. Furans and aromatics were the main products of cellulose under the activity of ZSM-5 Carlson et al. 2009 Lazaridis et al. 2018).

The Py-GC/MS partial pyrolysis test products of cellulose pyrolysis without catalyst are listed in the supplementary materials (Table **S1**). After adding the catalyst ZSM-5, the cellulose pyrolysis products

contain benzene and other hydrocarbons. Also, hydrocarbons, such as benzene, have increased dramatically, indicating that a large number of hydrodeoxygenation reactions occurred in cellulose pyrolysis under the catalysis of the zeolite catalyst ZSM-5, which improves the quality of bio-oil Zhou et al. 2014 . Also, the content of carbohydrates and furans was relatively reduced slightly, as cellulose might become pyrolyzed more intensely under the effect of ZSM-5, and carbohydrates and furans were further pyrolyzed into other substances with small molecules. Based on the above facts, we further explored the catalytic pyrolysis mechanisms of cellulose under the action of ZSM-5 based on DFT quantum chemical calculations to better understand the catalytic pyrolysis mechanism of terrestrial biomass Gumidyala et al. 2016 . Besides, the corresponding product yields (for example, benzenes and furans) can be increased through specific reaction paths, which can be used as an essential means of producing chemical raw materials, which helps future studies.

Mechanism of ZSM-5 catalytic pyrolysis of cellulose by DFT

Possible reaction pathways of typical products of catalytic pyrolysis of cellulose

According to previous reports Zheng et al. 2016 Guo et al. 2019 Mettler et al. 2012 and the PY-GC/MS experimental results of current work, the main products' pathways (5-hydroxymethylfurfural, furfural, and benzene) in the cellulose catalytic pyrolysis reaction pathway were proposed. Hu et al. Hu et al. 2018 suggested a complete reaction route for the non-catalytic route of preparing 5-hydroxymethyl furfural and furfural from the pyrolysis of glucose as a model compound. The routes with the most significant probability of occurrence are shown in **Fig3**. The reaction of reactant (R) to 5-hydroxymethylfurfural (P_1) is path **1**, and the reaction of reactant (R) to furfural (P_2) is path **2-1**. However, this article mainly studies the mechanisms of catalytic pyrolysis. To reduce the simulation calculation error, we choose a calculation method that takes the weak interaction force between molecules into the functional—M06-2X. Then, based on the 6-31g(d) level and the temperature, the non-catalytic Gibbs free energy without catalyst participating in the reaction was calculated. The transition states of the elementary reactions are listed in the supplementary information Table **2**.

Path **1** (yellow) is a typical path where D-fructose (DF) participates. Glucose first undergoes a ring-opening reaction to form acyclic D-glucose (IM_1) with the activation free energy of 8.9 kcal/mol. This reaction involves a coordinated transition state, TS_1 (Table **2**). IM_1 is re-isomerized to DF (IM_2), with the activation free energy of 72.8 kcal/mol. This reaction involves a coordinated transition state, TS_2 (Table **2**), in which the 2-hydroxy H was transferred to the 1-carbonyl group, and the other H in the C2 position is transferred to the C1 position. Later, DF formed β-D-fructofuranose (IM_3) by forming a transition state TS_3 in the form of a 2,5-acetal ring (Table **2**). The quaternary transition state TS4 dehydrates IM3 at 2-OH+1-H (hydroxyl at C2 position and hydrogen at C1 position) to form intermediate IM_4 (ΔEa = 89.9 kcal/mol), which is the decisive rate of the reaction path step. IM_4 undergoes one-step of electro-ring dehydration to form IM5 directly. The reaction is a six-membered transition state TS_5 (Table **2**), where 3-OH and 1-H (OH) are dehydrated, and C2=C3 bonds and C1=O bonds are formed. The reaction is thermodynamically

favorable (ΔG = −25.2 kcal/mol) and requires relatively low activation energy (ΔEa = 34 kcal/mol). Finally, IM_5 dehydrates at the 4-OH + 5-H site to form 5-HMF (P_1).

Path **2-1** is the most advantageous way for 3-deoxy-glucosone (3-DG) to participate in FF formation. As shown in **Fig3**, IM_1 is first dehydrated at the 3-OH+2-H site to form the enol isomer IM_6 of 3-DG (IM_1-TS_7, ΔEa = 63 kcal/mol). Then IM_6 undergoes enol-ketone tautomerism through the quaternary transition state TS_8 (IM_6-TS_8, ΔEa = 70.1 kcal/mol) into 3-DG (IM_7). Both of these reactions are thermodynamically favorable (ΔG = −18.2 and -0.5 kcal/mol). Similar to DF, 3-DG forms a 2,5-acetal ring through hemiacetal reaction to form a five-membered intermediate IM_8. The formation of IM_8 involves the quaternary transition state TS_9, the structure of which is shown in Table **2**. In Path **2-1** (blue), IM_8 is dehydrated between 4-OH and 6-H (OH) and formaldehyde to form an intermediate product IM_9 with a high activation free energy of 84.3 kcal/mol. This is the decisive step of path **2-1**. The reaction involves the six-membered transition state TS_{10}, the structure of which is shown in Table **2**. Finally, IM_9 is dehydrated at the 2-OH + 3-H site to form FF (P_2). The acyclic D-glucose produced by the ring-opening reaction of β-D-glucopyranose, and DF and 3-DG as important intermediates, are essential for developing both 5-HMF and FF.

After DF and 3-DG were formed in Path **1** and Path **2-1**, respectively, the five-membered intermediate could quickly form 5-HMF and FF through a continuous dehydration reaction. Since the boiling point of 5-HMF is 114~116℃, but the experimental temperature is 550℃. Therefore, under rapid high-temperature pyrolysis, 5-HMF will be further degraded. Degradation products include furans (5-methylfurfural, furfural, 2-methylfuran, etc.) and small molecules (CO, CO_2, H_2O, formic acid, formaldehyde, acetic acid, etc.). Therefore, we consider the reaction of P_1 to directly remove formaldehyde through transition state TS_{12} to obtain P_2 as path **2-2** (red). This process of eliminating formaldehyde requires activation-free energy of 85.5 kcal/mol.

According to our experimental results, after adding the zeolite catalyst, new aromatic products (benzene, toluene, p-xylene, etc.) appeared in the product. Some researchers have proposed that furan compounds will undergo DA cycloaddition reaction with olefins, and furfural will undergo decarbonylation to produce carbon monoxide and furan Cheng and Huber 2012 . For this reason, we propose a conversion path from furfural (P_2) to benzene (P_3) on this basis, as shown in **Fig3**, path **3** (orange). Furfural first removes free carbon monoxide through the transition state TS_{13} to form the furan intermediate IM_{10}. This is the crucial step of the path, which requires activation free energy of 88.2 kcal/mol. During the reaction, IM_{10} and short-chain ethylene undergo a DA reaction (IM_{10}-TS_{14}, ΔEa=70.1 kcal/mol) to obtain intermediate IM_{11}. Under the reaction of water molecules, the C4-O ether bond of IM_{11} together with the C2=C3 double bond are disturbed. Then, a new C3=C4 double bond is generated, and a C1-C2-O ether bond is generated to obtain a ternary epoxy structure. Finally, a hydrogen bond is formed between the hydrogen of the water molecule and the epoxy, resulting in the IM12 complex. This reaction requires activation free energy of

74.2 kcal/mol. However, the IM_{12} intermediate has a shorter residence time and is quickly isomerized to IM_{13}. IM_{13} continuously removes two molecules of water to obtain the product benzene (P_3).

The energy consumed by the non-catalytic reaction path was generally at a high level. The easiest way to reduce the reaction energy barrier is to add a catalyst, and the experimental results also confirm the yield gap of typical products in the pyrolysis reaction after adding the catalyst (Table **3**). Next, by calculating the reaction's energy after adding the catalyst, we will explain the changes in the product yield from a theoretical point of view.

Possible reaction pathways of typical products of cellulose catalytic pyrolysis

In the catalytic reaction system, the reactant and the catalyst interact. To express the reaction energy more accurately and reduce the calculation error, we put the reactant and the catalyst in the same system for simulation. Therefore, add the prefix C_ when naming each compound. When the compound is close to the acidic site of the catalyst, a complex is formed, where this adsorption process has certain adsorption energy. Since adsorption has little effect on product selectivity, this article ignores the effect of adsorption.

Qian et al. found that the 2-OH protonation on D-glucose resulted in the formation of 5-HMF and furfural through carbocation rearrangement Qian et al. 2005 . The protonation of 3-OH and 4-OH leads to two different five-membered ring degradation products in addition to 5-HMF, which may be the reason for other non-cellulose materials observed in experiments Abatzoglou et al. 1986 Qian et al. 2005 . However, the protonation of 1-OH and 6-OH does not cause any observable reactions. The Multiwfn software was used to predict and analyze the surface electrostatic potential of glucose molecules. As shown in Table **4**, the 3-OH of R was the most active (-40.2 kcal/mol), followed by the 4-OH position. Also, the active-H of the catalyst was an acidic site. Considering all together, we choose the 4-OH site on R to react with the catalyst first. Therefore, a catalytic pyrolysis path from D-glucose to 5-HMF was designed, as shown in **Fig4**.

Table 4. Extreme value of the electrostatic potential on the surface of glucose molecule.

Number of surface minima: 7			
#	a.u.	eV	kcal/mol
1 2-OH	-0.03936667	-1.071222	-24.702979
2 4-OH	-0.06223913	-1.693613	-39.055676
3* 3-OH	-0.06403766	-1.742553	-40.18427
4 C1-O7-C5	-0.03468574	-0.943847	-21.765646
5 1-OH	-0.04740712	-1.290013	-29.74844
6 C6-H	0.02659904	0.723797	16.691161
7 6-OH	0.01467596	0.399353	9.209311

Table **5** lists the transition state geometry involved in the catalytic pyrolysis. In path **1'**(pink), C_R generates C_IM_1 through the dehydration of transition state C_TS_1, with the activation free energy of 2.2 kcal/mol. In this elementary reaction, the active site active-H of the catalyst was close to the 4-OH on the ring leading to dehydration. At the same time, 5-H, is returned to the catalyst to form the six-member epoxy olefin intermediate IM_1. The second step was the ring-opening reaction. Active-H induces the breaking of the ether bond on the ring, forming 5-OH of the linear intermediate IM_2. Also, 1-OH provides an H atom to the catalyst to form 1-carbonyl group; IM_1 generates intermediate IM_2, with the activation energy of 1.9 kcal/mol. The third step is the hydrogen transfer reaction. In the presence of a catalyst, the carbonyl group is attacked by active hydrogen, 2-H is transferred to the C1 position, and 2-OH gives a hydrogen atom. The activation free energy from IM_2 to C_TS_3 is 4.7 kcal/mol. In the absence of a catalyst, the fourth step is an aldol condensation reaction, but it is easier to induce ring formation by active-H atoms. The straight-chain needs to be rotated and bent to form a ring, while the catalyst's porous structure promotes the straight-chain to bend; resulting in a shorter distance between the 2-carbonyl group and the 5-hydroxy group. When the space structure is suitable, active-H attacks the 2-carbonyl group, and the 5-OH breaks away from hydrogen and returns to the catalyst. This condensation reaction forms the furan ring precursor intermediate IM_4 through the transition state C_TS_4 (ΔEa = 6.7 kcal/mol). Subsequently, IM_4 is dehydrated at 2-OH+active-H and 1-H (OH)+C and forms a C2=C3 bond. An 18.4 kcal/mol activation energy was consumed in the process of forming the enol intermediate IM_5. Finally, IM_5 can directly undergo cyclization dehydration tautomerization reaction to form P_1 in one step. The reaction is the ten-membered transition state C_TS_6 (Table **5**), where 3-OH+active-H and 1-H (OH)+C are dehydrated and form C2=C3 and C1=O.

There are two paths for non-catalytic pyrolysis to generate P_2. We choose the shortest path (path **2-2'**, green) to calculate catalytic pyrolysis's energy; P_1 removes the terminal free methylene group. The active H of the catalyst promotes the breaking of the C5-C6 single bond, the methylene group is then separated from the furan ring, and then the active hydrogen is added to the C4=C5 double bond. The hydroxyl group

of -CH_2OH removes a hydrogen atom to neutralize the catalyst to maintain charge neutrality. The transition state C_TS_7 is shown in Table **5**. This formaldehyde removal process requires activation free energy of 35.3 kcal/mol, which is 50.2 kcal/mol lower than that of non-catalysis.

In the process where furfural reacts with ethylene to convert to benzene (path **3'**, purple), the catalyst has the same effect, and the catalytic reaction is induced by active hydrogen. The free 1-carbonyl group of furfural removes CO under the catalysis of active hydrogen. First, active-H attacks the C1-C2 positions to promote single bond cleavage. Subsequently, the reactive H undergoes an electrophilic attack to produce the intermediate furan (IM_6). At the same time, 1-H is returned to the catalyst and forms free CO. The second step Diels-Alder (DA) reaction, is the key step for forming benzene ring. Since the addition reaction is bimolecular, the transition state C_TS_9 with a roof-shaped spatial geometry is formed during the addition process. A double bond forms, so active-H cannot participate in the reaction, but active H affects the electronic structure around the reactant and can also reduce the energy required for the reaction to a certain extent, which is consistent with the report by Patet et al. Patet et al. 2017 . The third step is that active-H promotes the breaking of the ether bond and the free water molecules in the reaction process, and the oxygen on the ring form a hydrogen bond, preparing for the water addition reaction in the fourth step. Finally, two molecules of water are continuously removed to produce benzene (P_3). Table **6** lists the activation energy and reaction heat of the reaction process. **Fig7** is the potential energy curve of the non-catalytic and catalytic pathways for forming a benzene ring. We found that in non-catalysis, the decisive step is the first step of CO removal reaction. In catalysis, the final step is the DA reaction, and except for the DA reaction, the energy barrier of other elementary reactions is greatly reduced. This is all due to the excellent catalytic effect of the zeolite catalyst. It also shows that the effect of zeolite catalyst on the DA reaction is not favorable. Since the zeolite catalyst could not significantly reduce the energy required for DA reaction. We will further explore high-efficiency catalysts to reduce the DA reaction's energy barrier in the future study.

Table 6. Kinetic and thermodynamic parameters of cellulose catalytic pyrolysis reaction pathway (kcal/mol).

	Activation energy (ΔEa)	Reaction heat (ΔG)
Path **1'**		
R- ts1- im1	2.18	-8.82
im1- ts2- im2	1.86	-5.98
im2- ts3- im3	4.73	3.35
im3- ts4- im4	6.66	-5.74
im4- ts5- im5	18.35	-11.72
im5- ts6- P1	5.30	-25.57
Path **2'**		
P1- ts7- P2	35.28	15.44
Path **3'**		
P2- ts8- im6	2.17	-17.41
im6- ts9- im7	45.35	2.25
im7- ts10- im8	26.70	11.16
im8- ts11- im9	15.80	-12.66
im9- ts12- im10	27.01	-17.07
im10- ts13- P3	1.42	-26.24

Fig8 shows the potential energy curves of different catalytic pathways. In the catalytic reaction, each step of the reaction's activation free energy is greatly reduced, which is very beneficial to the reaction in terms of kinetics. The reaction heat of the non-catalyzed reaction is in the supporting information Table **S1**, and the reaction heat of the catalyzed reaction is listed in Table **6**. The thermodynamic energy of most elementary reactions is negative, representing an exothermic process, which is also thermodynamically beneficial. We also found that most of the transition states involved in non-catalytic reactions are four-membered ring transition states. Still, the eight-membered transition state dominates the transition states of catalytic reactions, and there is also the ten-membered transition state C_TS_6. Also, C_TS_6 has the lowest activation energy of transition state structure in all dehydration reactions, which is only 5.3 kcal/mol. If the transition state ring formed at the position where the chemical reaction occurs is larger, the activation energy required for the reaction is less. This is consistent with our previous research results Wang et al. 2021 Cheng et al. 2021 .

The speed-determining steps of the three catalytic pathways are C_TS_5 ($\Delta Ea_{path1'\text{-}L}$=18.4 kcal/mol), C_$TS_7$ ($\Delta Ea_{path2\text{-}2'\text{-}L}$=35.3 kcal/mol), and C_$TS_9$ ($\Delta Ea_{path3'\text{-}L}$=45.4 kcal/mol), indicating that 5-hydroxymethyl furfural is the easiest to produce from glucose, followed by furfural, and finally benzene.

In the experiment, cellulose was first decomposed into single-molecule glucose, and then the glucose had 5-hydroxymethylfurfural, furfural, and benzene according to the difficulty of the reaction. Moreover, benzene can only be produced when the catalyst is present. In the non-catalytic pyrolysis experiment, the yield of furfural reached 25.34%, while after adding the catalyst, it decreased to 12.81%. However, the content of benzene increased from almost zero to 13.04%. Therefore, it can be inferred that furfural participates in the production of benzene, showing that the experimental and theoretical results are consistent.

To study the Diels-Alder cycloaddition reaction of furan and ethylene on the Brønsted-acidic molecular sieve, Patet et al. used electronic structure calculations and microscopic kinetic models, and the subsequent dehydration reaction of furan and ethylene Patet et al. 2017 . The electronic structure calculation showed that the acid strength of the Brønsted-acidic zeolite changes with the changes of Al, Ga, Fe, and B metal substituents. For these four modified Brønsted-acidic zeolites, the catalytic effect of the DA reaction is not apparent. However, for dehydration reactions, Brønsted-acidic follows the general principle of acid catalysis for dehydration reactions and plays an essential role in catalyzing these reactions. Our calculation results also showed that the activation energy of the DA reaction catalyzed by zeolite was 45.4 kcal/mol, which is only 9.4 kcal/mol lower than the uncatalyzed activation energy. However, the dehydration reaction's activation energy is reduced by about 40-70 kcal/mol. Therefore, we suggest that steric hindrance may make the DA cycloaddition reaction more complex, so the change in acid strength shows an extensive role in catalysis.

Conclusion

In this study, density functional theory was used to study the Py-GC/MS experiment of fast pyrolysis of cellulose and its thermal decomposition mechanism. Combining the experimental results, this paper proposes several reaction pathways for the catalytic pyrolysis reaction mechanism of cellulose. Compared with the results of cellulose monomolecular pyrolysis, under the catalysis of the zeolite catalyst ZSM-5, many deoxygenation reactions occurred during the cellulose pyrolysis process. The role of hydrogen bonds improves the quality of bio-oil, and effectively reduces the reaction's energy barrier, which makes the pyrolysis reaction of cellulose easier to occur. According to the degree of difficulty of the reaction (the energy barrier of the speed-determining step and the heat of reaction of the reaction process), glucose sequentially generates 5-hydroxymethylfurfural, furfural and benzene, and the benzene ring can only be formed when the zeolite catalyst is present. The relatively low content of carbohydrates and furans may be due to the higher intensity of cellulose's catalytic pyrolysis. For example, furan compounds will be further decomposed into other small molecules. Moreover, ZSM-5 directly participates in most of the pyrolysis reaction of cellulose, where the electrophilicity of acidic sites in the reaction system plays an important role. Therefore, the catalyst's addition significantly reduces the energy barrier of each path in the pyrolysis reaction. The dehydration reaction can be fully catalyzed, the activation energy of the reaction is reduced, and the formation of aromatic compounds were promoted. However, due to the steric hindrance of the Diels-Alder cycloaddition reaction, the energy barrier of the rate-determining step of converting furan compounds to aromatics is relatively small. The catalyst can lower

the reaction energy barrier; the more active sites of the catalyst, the faster the reaction rate, which provides useful guidance to select a suitable catalyst for the dehydration and aromatization of furan compounds in order to produce aromatic compounds in experiments.

Declarations

I hereby declare that all the information contained in this resume is in accordance with facts or truths to my knowledge. I take full responsibility for the correctness of the said information.

Fund

The authors are grateful to the Key Research and Development Project of Jiangsu Province (BE2019009-4).

This study was funded by the Jiangsu Province “333 project” (BRA2019277).

This work was supported by the Foundation of State Key Laboratory of Coal combustion (FSKLCCA1904).

This research work is supported by the high-performance computing platform of Jiangsu University.

Conflicts of interest/Competing interests

The authors declare that they have no conflict of interest.

Availability of data and materials

The datasets used and analyzed during this article are availability from the corresponding author on reasonable requests.

Code availability

All calculations were performed on the Gaussian 09W program suite.

ChemDraw Pro 14.0 and Origin 2017 software are used for mechanism visualization and data mapping, respectively.

Multiwfn 3.7 for electrostatic potential analysis.

Authors’ contributions

Xiaoxue Cheng wrote the paper and produced the charts.

Ding Jiang supervised the calculation method of the paper and the review of the calculation data.

Zhen Xia was in charge of the Py-GC/MS experiment.

Bahram Barati and Karthickeyan Viswanathan are responsible for the correction of English grammar.

Yamin Hu,Lili Qian and Zhixia He supervised the experiment.

Shuang Wang guides the general idea of the article.

Hongping Li directs the design idea of calculation path.

Compliance with Ethical Standards

This paper does not contain any studies with human participants or animals performed by any of the authors.

Acknowledgements

The authors are grateful to the Key Research and Development Project of Jiangsu Province (BE2019009-4), the Jiangsu Province “333 project” (BRA2019277), the Foundation of State Key Laboratory of Coal combustion (FSKLCCA1904). This research work is supported by the high-performance computing platform of Jiangsu University.

References

1. Wang S., Xia Z., Wang Q., He Z., Li H. 2017 Mechanism research on the pyrolysis of seaweed polysaccharides by Py-GC/MS and subsequent density functional theory studies. J Anal Appl Pyrolysis 126: 118-131. https://doi.org/10.1016/j.jaap.2017.06.018
2. Alvarez J., Lopez G., Amutio M., Bilbao J., Olazar M. 2014 Bio-oil production from rice husk fast pyrolysis in a conical spouted bed reactor. Fuel 128: 162-169. https://doi.org/10.1016/j.fuel.2014.02.074
3. Anastasakis K., Ross A.B., Jones J.M. 2011 Pyrolysis behaviour of the main carbohydrates of brown macro-algae. Fuel 90: 598-607. https://doi.org/10.1016/j.fuel.2010.09.023
4. Wang S., Chen J., Cai Q., Zhang F., Wang Y., Ru B., Wang Q. 2016 The effect of mild hydrogenation on the catalytic cracking of bio-oil for aromatic hydrocarbon production. Int J Hydrogen Energy 41: 16385-16393. https://doi.org/10.1016/j.ijhydene.2015.12.024
5. Zeng M., Pan X. 2020 Insights into solid acid catalysts for efficient cellulose hydrolysis to glucose: progress, challenges, and future opportunities. Catal. Rev.: Sci. Eng. 64: 781-786. https://doi.org/10.1080/01614940.2020.1819936
6. Hu B., Zhang B., Xie W.-l., Jiang X.-y., Liu J., Lu Q. 2020 Recent Progress in Quantum Chemistry Modeling on the Pyrolysis Mechanisms of Lignocellulosic Biomass. Energy Fuels 34: 10384–10440. https://doi.org/10.1021/acs.energyfuels.0c01948

7. Sharma A., Pareek V., Zhang D. 2015 Biomass pyrolysis—A review of modelling, process parameters and catalytic studies. Renewable Sustainable Energy Rev. 50: 1081-1096. https://doi.org/10.1016/j.rser.2015.04.193
8. Shen D., Jin W., Hu J., Xiao R., Luo K. 2015 An overview on fast pyrolysis of the main constituents in lignocellulosic biomass to valued-added chemicals: Structures, pathways and interactions. Renewable Sustainable Energy Rev. 51: 761-774. https://doi.org/10.1016/j.rser.2015.06.054
9. Jiang D., Li J., Wang S., Li H., Qian L., Li B., Cheng X., Hu Y., Hu X. 2020 Cyclic Compound Formation Mechanisms during Pyrolysis of Typical Aliphatic Acidic Amino Acids. ACS Sustainable Chem. Eng. 8: 16968-16978. https://doi.org/10.1021/acssuschemeng.0c07108
10. Wang S., Wang Q., Jiang X., Han X., Ji H. 2013 Compositional analysis of bio-oil derived from pyrolysis of seaweed. Energy Convers Manage 68: 273-280. https://doi.org/10.1016/j.enconman.2013.01.014
11. Xu S., Cao B., Uzoejinwa B.B., Odey E.A., Wang S., Shang H., Li C., Hu Y., Wang Q., Nwakaire J.N. 2020 Synergistic effects of catalytic co-pyrolysis of macroalgae with waste plastics. Process Saf Environ Prot 137: 34-48. https://doi.org/10.1016/j.psep.2020.02.001
12. Yuan C., Jiang D., Wang S., Barati B., Gong X., Cao B., Zhang R., Zhang C., Odey E.A. 2020 Study on catalytic pyrolysis mechanism of seaweed polysaccharide monomer. Combust Flame 218: 1-11. https://doi.org/10.1016/j.combustflame.2020.04.022
13. Banerjee A., Mushrif S.H. 2017 Reaction Pathways for the Deoxygenation of Biomass-Pyrolysis-Derived Bio-oil on Ru: A DFT Study using Furfural as a Model Compound. ChemCatChem 9: 2828-2838. https://doi.org/10.1002/cctc.201700036
14. Moazeni F., Chen Y.-C., Zhang G. 2019 Enzymatic transesterification for biodiesel production from used cooking oil, a review. J. Cleaner Prod. 216: 117-128. https://doi.org/10.1016/j.jclepro.2019.01.181
15. Rathnayake M., Chaireongsirikul T., Svangariyaskul A., Lawtrakul L., Toochinda P. 2018 Process simulation based life cycle assessment for bioethanol production from cassava, cane molasses, and rice straw. J. Cleaner Prod. 190: 24-35. https://doi.org/10.1016/j.jclepro.2018.04.152
16. Wang S., Dai G., Yang H., Luo Z. 2017 Lignocellulosic biomass pyrolysis mechanism: A state-of-the-art review. Prog Energy Combust Sci 62: 33-86. https://doi.org/10.1016/j.pecs.2017.05.004
17. Zeng K., Li J., Xie Y., Yang H., Yang X., Zhong D., Zhen W., Flamant G., Chen H. 2020 Molten salt pyrolysis of biomass: The mechanism of volatile reforming and pyrolysis. Energy 213: 118801. https://doi.org/10.1016/j.energy.2020.118801
18. Torri I.D.V., Paasikallio V., Faccini C.S., Huff R., Caramão E.B., Sacon V., Oasmaa A., Zini C.A. 2016 Bio-oil production of softwood and hardwood forest industry residues through fast and intermediate pyrolysis and its chromatographic characterization. Bioresour Technol 200: 680-690. https://doi.org/10.1016/j.biortech.2015.10.086
19. Ding Y., Ezekoye O.A., Lu S., Wang C., Zhou R. 2017 Comparative pyrolysis behaviors and reaction mechanisms of hardwood and softwood. Energy Convers Manage 132: 102-

109. https://doi.org/10.1016/j.enconman.2016.11.016

20. Fan Y., Zhang D., Zheng A., Zhao Z., Li H., Yang T. 2019 Selective production of anhydrosugars and furfural from fast pyrolysis of corncobs using sulfuric acid as an inhibitor and catalyst. Chem Eng J 358: 743-751. https://doi.org/10.1016/j.cej.2018.10.014
21. Dai L., Wang Y., Liu Y., He C., Ruan R., Yu Z., Jiang L., Zeng Z., Wu Q. 2020 A review on selective production of value-added chemicals via catalytic pyrolysis of lignocellulosic biomass. Sci Total Environ 749: 142386. https://doi.org/10.1016/j.scitotenv.2020.142386
22. Chen J., Cai Q., Lu L., Leng F., Wang S. 2017 Upgrading of the Acid-Rich Fraction of Bio-oil by Catalytic Hydrogenation-Esterification. ACS Sustainable Chem. Eng. 5: 1073-1081. https://doi.org/10.1021/acssuschemeng.6b02366
23. Zhang S., Zhang H., Liu X., Zhu S., Hu L., Zhang Q. 2018 Upgrading of bio-oil from catalytic pyrolysis of pretreated rice husk over Fe-modified ZSM-5 zeolite catalyst. Fuel Process Technol 175: 17-25. https://doi.org/10.1016/j.fuproc.2018.03.002
24. Li X., Dong W., Zhang J., Shao S., Cai Y. 2020 Preparation of bio-oil derived from catalytic upgrading of biomass vacuum pyrolysis vapor over metal-loaded HZSM-5 zeolites. J. Energy Inst. 93: 605-613. https://doi.org/10.1016/j.joei.2019.06.005
25. Thangalazhy-Gopakumar S., Adhikari S., Chattanathan S.A., Gupta R.B. 2012 Catalytic pyrolysis of green algae for hydrocarbon production using H+ZSM-5 catalyst. Bioresour Technol 118: 150-157. https://doi.org/10.1016/j.biortech.2012.05.080
26. Lee H.W., Choi S.J., Park S.H., Jeon J.-K., Jung S.-C., Joo S.H., Park Y.-K. 2014 Catalytic conversion of Laminaria japonica over microporous zeolites. Energy 66: 2-6. https://doi.org/10.1016/j.energy.2013.05.023
27. Rahman M.M., Chai M., Sarker M., Nishu, Liu R. 2020 Catalytic pyrolysis of pinewood over ZSM-5 and CaO for aromatic hydrocarbon: Analytical Py-GC/MS study. J. Energy Inst. 93: 425-435. https://doi.org/10.1016/j.joei.2019.01.014
28. Nishu, Liu R., Rahman M.M., Sarker M., Chai M., Li C., Cai J. 2020 A review on the catalytic pyrolysis of biomass for the bio-oil production with ZSM-5: Focus on structure. Fuel Process Technol 199: 106301. https://doi.org/10.1016/j.fuproc.2019.106301
29. Wu S., Shen D., Hu J., Xiao R., Zhang H. 2013 TG-FTIR and Py-GC–MS analysis of a model compound of cellulose – glyceraldehyde. J Anal Appl Pyrolysis 101: 79-85. https://doi.org/10.1016/j.jaap.2013.02.009
30. Yang X., Zhao Y., Li R., Wu Y., Yang M. 2018 A modified kinetic analysis method of cellulose pyrolysis based on TG–FTIR technique. Thermochim Acta 665: 20-27. https://doi.org/10.1016/j.tca.2018.05.008
31. Lu Q., Zhou M.-x., Li W.-t., Wang X., Cui M.-s., Yang Y.-p. 2018 Catalytic fast pyrolysis of biomass with noble metal-like catalysts to produce high-grade bio-oil: Analytical Py-GC/MS study. Catal Today 302: 169-179. https://doi.org/10.1016/j.cattod.2017.08.029

32. Chen H., Xie Y., Chen W., Xia M., Li K., Chen Z., Chen Y., Yang H. 2019 Investigation on co-pyrolysis of lignocellulosic biomass and amino acids using TG-FTIR and Py-GC/MS. Energy Convers Manage 196: 320-329. https://doi.org/10.1016/j.enconman.2019.06.010
33. Dai G., Wang S., Zou Q., Huang S. 2018 Improvement of aromatics production from catalytic pyrolysis of cellulose over metal-modified hierarchical HZSM-5. Fuel Process Technol 179: 319-323. https://doi.org/10.1016/j.fuproc.2018.07.023
34. Yang M., Shao J., Yang H., Zeng K., Wu Z., Chen Y., Bai X., Chen H. 2019 Enhancing the production of light olefins and aromatics from catalytic fast pyrolysis of cellulose in a dual-catalyst fixed bed reactor. Bioresour Technol 273: 77-85. https://doi.org/10.1016/j.biortech.2018.11.005
35. Shen Y., Wang S., Huang S., Li Z., Ma X. 2014 DFT investigations of the reaction mechanism of diethyl carbonate synthesis catalyzed by Cu(I)/β or Pd(II)/β zeolites. Appl Surf Sci 308: 237-246. https://doi.org/10.1016/j.apsusc.2014.04.141
36. Alves M., Méreau R., Grignard B., Detrembleur C., Jérôme C., Tassaing T. 2017 DFT investigation of the reaction mechanism for the guanidine catalysed ring-opening of cyclic carbonates by aromatic and alkyl-amines. RSC Adv. 7: 18993-19001. https://doi.org/10.1039/C7RA00220C
37. Shen Y., Meng Q., Huang S., Gong J., Ma X. 2013 DFT investigations for the reaction mechanism of dimethyl carbonate synthesis on Pd(II)/beta zeolites. Phys Chem Chem Phys 15: 13116-13127. https://doi.org/10.1039/C3CP51092A
38. Lin Y.-C., Cho J., Tompsett G.A., Westmoreland P.R., Huber G.W. 2009 Kinetics and Mechanism of Cellulose Pyrolysis. J. Phys. Chem. C 113: 20097-20107. https://doi.org/10.1021/jp906702p
39. Zhang M., Geng Z., Yu Y. 2015 Density Functional Theory (DFT) study on the pyrolysis of cellulose: The pyran ring breaking mechanism. Comput. Theor. Chem. 1067: 13-23. https://doi.org/10.1016/j.comptc.2015.05.001
40. Zhang M., Geng Z., Yu Y. 2011 Density Functional Theory (DFT) Study on the Dehydration of Cellulose. Energy Fuels 25: 2664-2670. https://doi.org/10.1021/ef101619e
41. Zhang Y., Liu C., Chen X. 2015 Unveiling the initial pyrolytic mechanisms of cellulose by DFT study. J Anal Appl Pyrolysis 113: 621-629. https://doi.org/10.1016/j.jaap.2015.04.010
42. Lu Q., Tian H.-y., Hu B., Jiang X.-y., Dong C.-q., Yang Y.-p. 2016 Pyrolysis mechanism of holocellulose-based monosaccharides: The formation of hydroxyacetaldehyde. J Anal Appl Pyrolysis 120: 15-26. https://doi.org/10.1016/j.jaap.2016.04.003
43. Cao B., Yuan J., Jiang D., Wang S., Barati B., Hu Y., Yuan C., Gong X., Wang Q. 2021 Seaweed-derived biochar with multiple active sites as a heterogeneous catalyst for converting macroalgae into acid-free biooil containing abundant ester and sugar substances. Fuel 285: 119-164. https://doi.org/10.1016/j.fuel.2020.119164
44. Liu C., Huang J., Huang X., Li H., Zhang Z. 2011 Theoretical studies on formation mechanisms of CO and CO2 in cellulose pyrolysis. Comput. Theor. Chem. 964: 207-212. https://doi.org/10.1016/j.comptc.2010.12.027

45. Chen K., Abdolrahmani M., Horstmeier S., Pham T.N., Nguyen V.T., Zeets M., Wang B., Crossley S., White J.L. 2019 Brønsted–Brønsted Synergies between Framework and Noncrystalline Protons in Zeolite H-ZSM-5. ACS Catal. 9: 6124-6136. https://doi.org/10.1021/acscatal.9b01583
46. Dumrongsakda P., Ruangpornvisuti V. 2012 Theoretical Investigation of Ethanol Conversion to Ethylene over H–ZSM–5 and Transition Metals–Exchanged ZSM–5. Catal Lett 142: 143-149. https://doi.org/10.1007/s10562-011-0737-5
47. Reina M., Martinez A., Cammarano C., Leroi C., Hulea V., Mineva T. 2017 Conversion of Methyl Mercaptan to Hydrocarbons over H-ZSM-5 Zeolite: DFT/BOMD Study. ACS Omega 2: 4647-4656. https://doi.org/10.1021/acsomega.7b00756
48. Frisch M.J., Trucks G.W., Schlegel H.B., Scuseria G.E., Robb M.A., Cheeseman J.R., Scalmani G., Barone V., Petersson G.A., Nakatsuji H., Li X., Caricato M., Marenich A.V., Bloino J., Janesko B.G., Gomperts R., Mennucci B., Hratchian H.P., Ortiz J.V., Izmaylov A.F., Sonnenberg J.L., Williams, Ding F., Lipparini F., Egidi F., Goings J., Peng B., Petrone A., Henderson T., Ranasinghe D., Zakrzewski V.G., Gao J., Rega N., Zheng G., Liang W., Hada M., Ehara M., Toyota K., Fukuda R., Hasegawa J., Ishida M., Nakajima T., Honda Y., Kitao O., Nakai H., Vreven T., Throssell K., Montgomery Jr. J.A., Peralta J.E., Ogliaro F., Bearpark M.J., Heyd J.J., Brothers E.N., Kudin K.N., Staroverov V.N., Keith T.A., Kobayashi R., Normand J., Raghavachari K., Rendell A.P., Burant J.C., Iyengar S.S., Tomasi J., Cossi M., Millam J.M., Klene M., Adamo C., Cammi R., Ochterski J.W., Martin R.L., Morokuma K., Farkas O., Foresman J.B., Fox D.J. 2016 Gaussian 16 Rev. B.01 Wallingford, CT Gaussian 16. https://gaussian.com/
49. Carlson T.R., Tompsett G.A., Conner W.C., Huber G.W. 2009 Aromatic Production from Catalytic Fast Pyrolysis of Biomass-Derived Feedstocks. Top Catal 52: 241. https://doi.org/10.1007/s11244-008-9160-6
50. Lazaridis P.A., Fotopoulos A.P., Karakoulia S.A., Triantafyllidis K.S. 2018 Catalytic Fast Pyrolysis of Kraft Lignin With Conventional, Mesoporous and Nanosized ZSM-5 Zeolite for the Production of Alkyl-Phenols and Aromatics. Front. Chem. 6: 295-295. https://doi.org/10.3389/fchem.2018.00295
51. Zhou G., Li J., Yu Y., Li X., Wang Y., Wang W., Komarneni S. 2014 Optimizing the distribution of aromatic products from catalytic fast pyrolysis of cellulose by ZSM-5 modification with boron and co-feeding of low-density polyethylene. Appl Catal, A 487: 45-53. https://doi.org/10.1016/j.apcata.2014.09.009
52. Gumidyala A., Wang B., Crossley S. 2016 Direct carbon-carbon coupling of furanics with acetic acid over Brønsted zeolites. Sci. Adv. 2: e1601072. https://doi.org/10.1126/sciadv.1601072
53. Zheng M., Wang Z., Li X., Qiao X., Song W., Guo L. 2016 Initial reaction mechanisms of cellulose pyrolysis revealed by ReaxFF molecular dynamics. Fuel 177: 130-141. https://doi.org/10.1016/j.fuel.2016.03.008
54. Guo S., Liang H., Che D., Liu H., Sun B. 2019 Quantitative study of the pyrolysis of levoglucosan to generate small molecular gases. RSC Adv. 9: 18791-18802. https://doi.org/10.1039/c9ra03138c
55. Mettler M.S., Mushrif S.H., Paulsen A.D., Javadekar A.D., Vlachos D.G., Dauenhauer P.J. 2012 Revealing pyrolysis chemistry for biofuels production: Conversion of cellulose to furans and small

oxygenates. Energy Environ. Sci. 5: 5414-5424. https://doi.org/10.1039/C1EE02743C

56. Hu B., Lu Q., Jiang X., Dong X., Cui M., Dong C., Yang Y. 2018 Pyrolysis mechanism of glucose and mannose: The formation of 5-hydroxymethyl furfural and furfural. J. Energy Chem. 27: 486-501. https://doi.org/10.1016/j.jechem.2017.11.013
57. Cheng Y.-T., Huber G.W. 2012 Production of targeted aromatics by using Diels–Alder classes of reactions with furans and olefins over ZSM-5. Green Chem 14: 3114-3125. https://doi.org/10.1039/C2GC35767D
58. Qian X., Nimlos M.R., Johnson D.K., Himmel M.E. 2005 Acidic sugar degradation pathways: an ab initio molecular dynamics study. Appl Biochem Biotechnol 121-124: 989-97. https://doi.org/10.1385/abab:124:1-3:0989
59. Abatzoglou N., Bouchard J., Chornet E., Overend R.J.C.J.C.E. 1986 Dilute acid depolymerization of cellulose in aqueous phase: experimental evidence of the significant presence of soluble oligomeric intermediates. Can J Chem Eng 64: 781-786. https://doi.org/10.1002/cjce.5450640510
60. Qian X., Nimlos M.R., Davis M., Johnson D.K., Himmel M.E. 2005 Ab initio molecular dynamics simulations of β-D-glucose and β-D-xylose degradation mechanisms in acidic aqueous solution. Carbohydr Res 340: 2319-2327. https://doi.org/10.1016/j.carres.2005.07.021
61. Patet R.E., Koehle M., Lobo R.F., Caratzoulas S., Vlachos D.G.J.T.J.o.P.C.C. 2017 General acid-type catalysis in the dehydrative aromatization of furans to aromatics in H-[Al]-BEA, H-[Fe]-BEA, H-[Ga]-BEA, and H-[B]-BEA zeolites. J. Phys. Chem. C 121: 13666-13679. https://doi.org/10.1021/acs.jpcc.7b02344
62. Wang S., Zhao S., Cheng X., Qian L., Barati B., Gong X., Cao B., Yuan C. 2021 Study on two-step hydrothermal liquefaction of macroalgae for improving bio-oil. Bioresour Technol 319: 124176. https://doi.org/10.1016/j.biortech.2020.124176
63. Cheng X., Jiang D., Hu X., Barati B., Hu Y., Qian L., He Z., Wang S., Li H. 2021 Mechanism of solvothermal conversion of xylose to furfural in rich-methanol solution: A study based on density functional theory. J Anal Appl Pyrolysis 154: 104996. https://doi.org/10.1016/j.jaap.2020.104996

Tables

Due to technical limitations, table 1, 2, 3 and 5 is only available as a download in the Supplemental Files section.

Figures

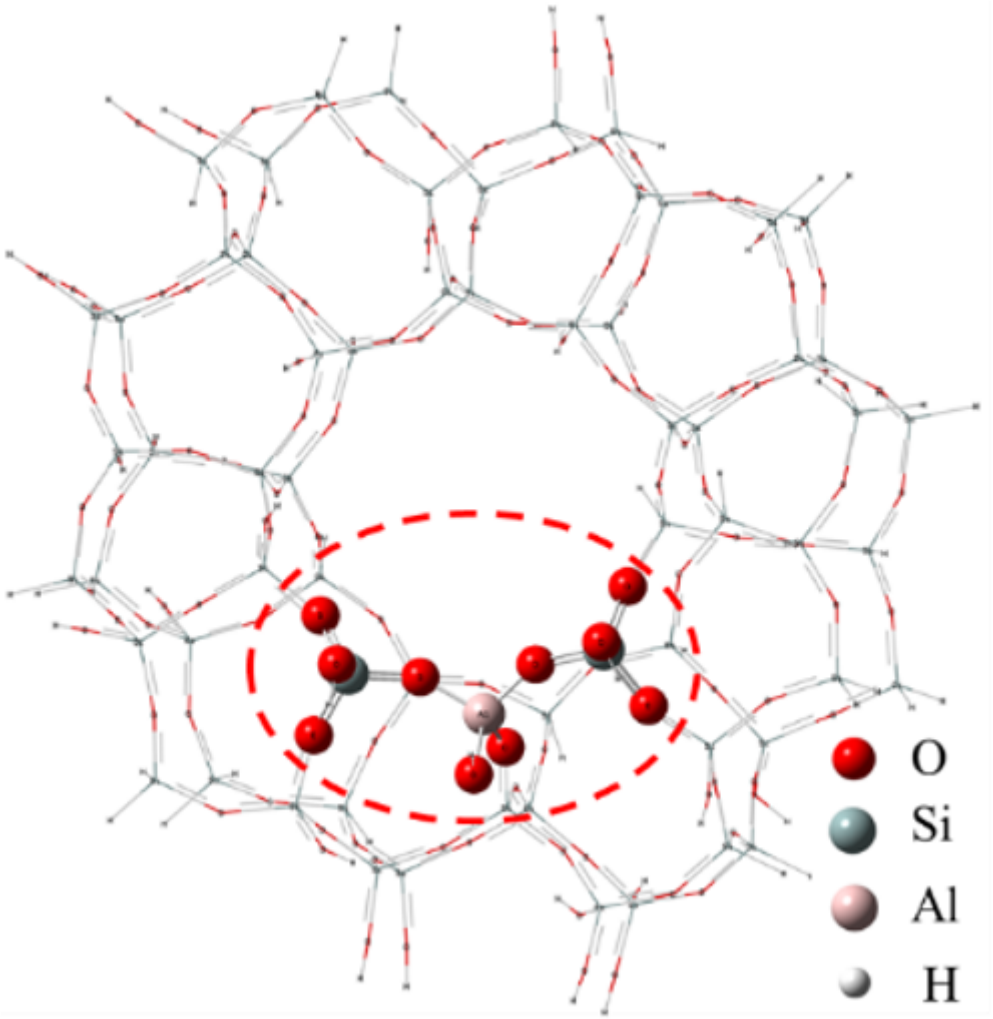

Figure 1

Simplified model of ZSM-5.

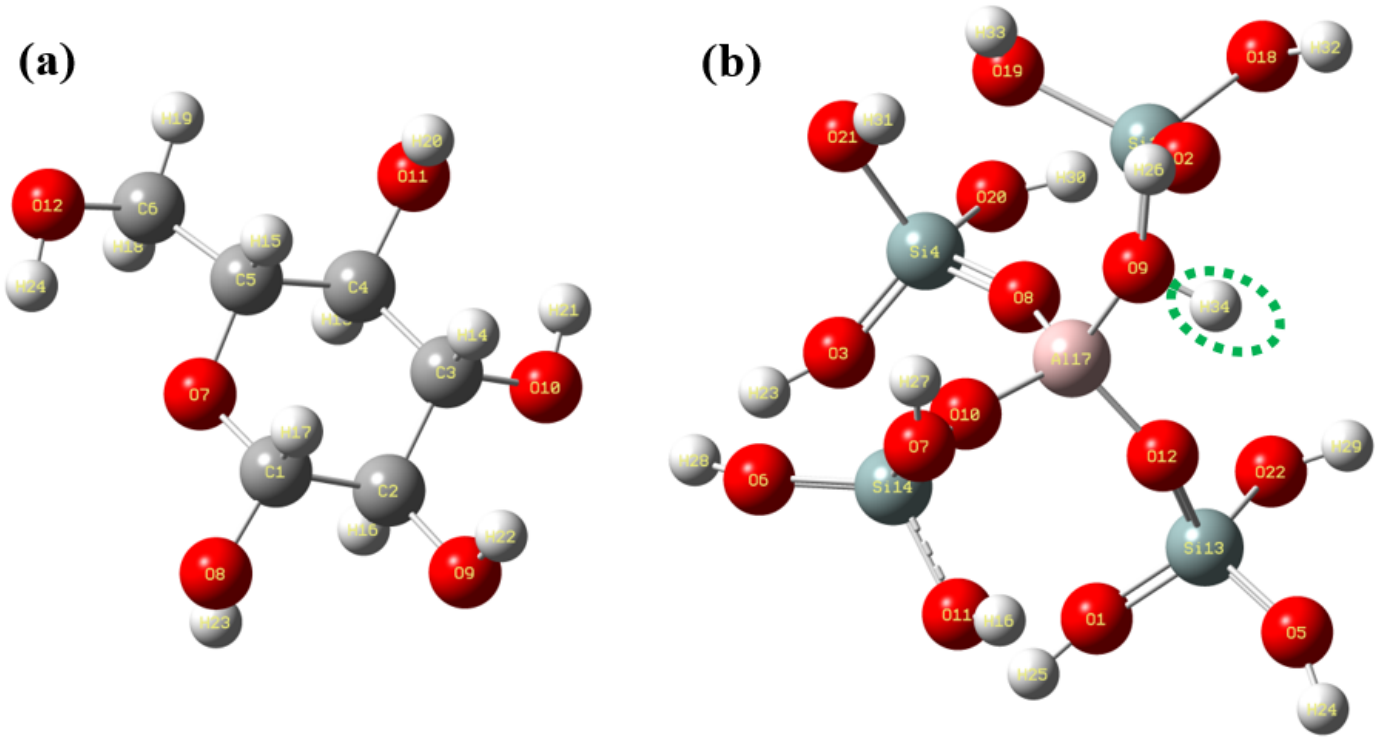

Figure 2

(a) The molecular structure of D-glucose; (b) The molecular structure of catalyst.

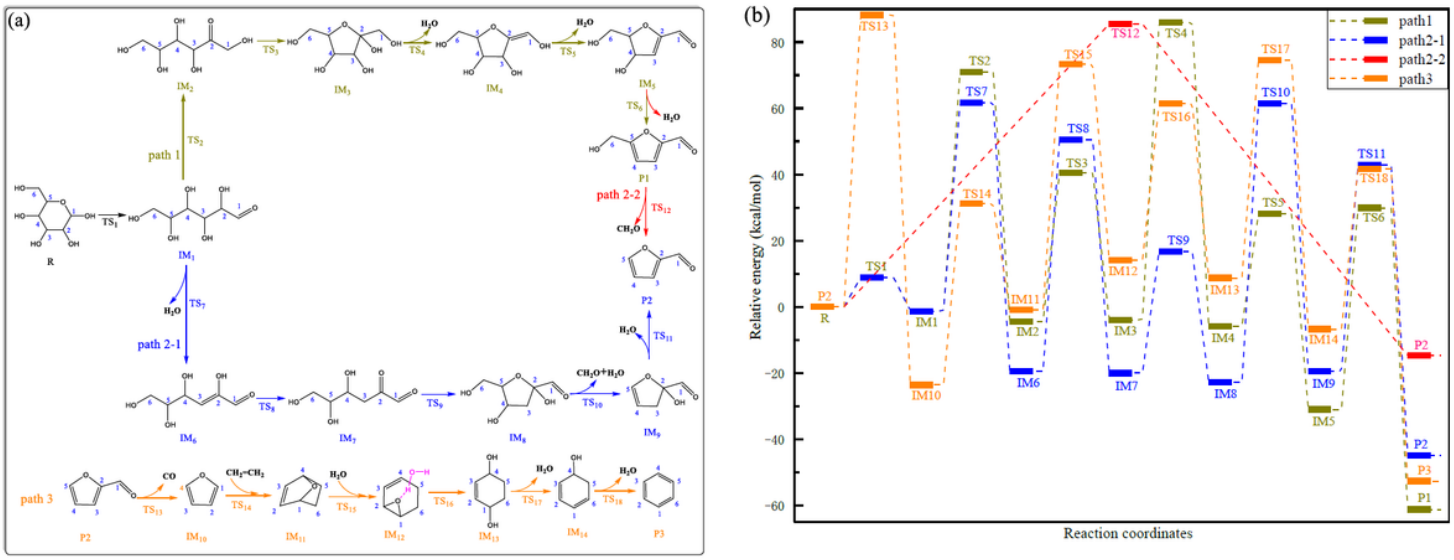

Figure 3

(a) Conversion path and (b) energy profiles of glucose non-catalytic pyrolysis.

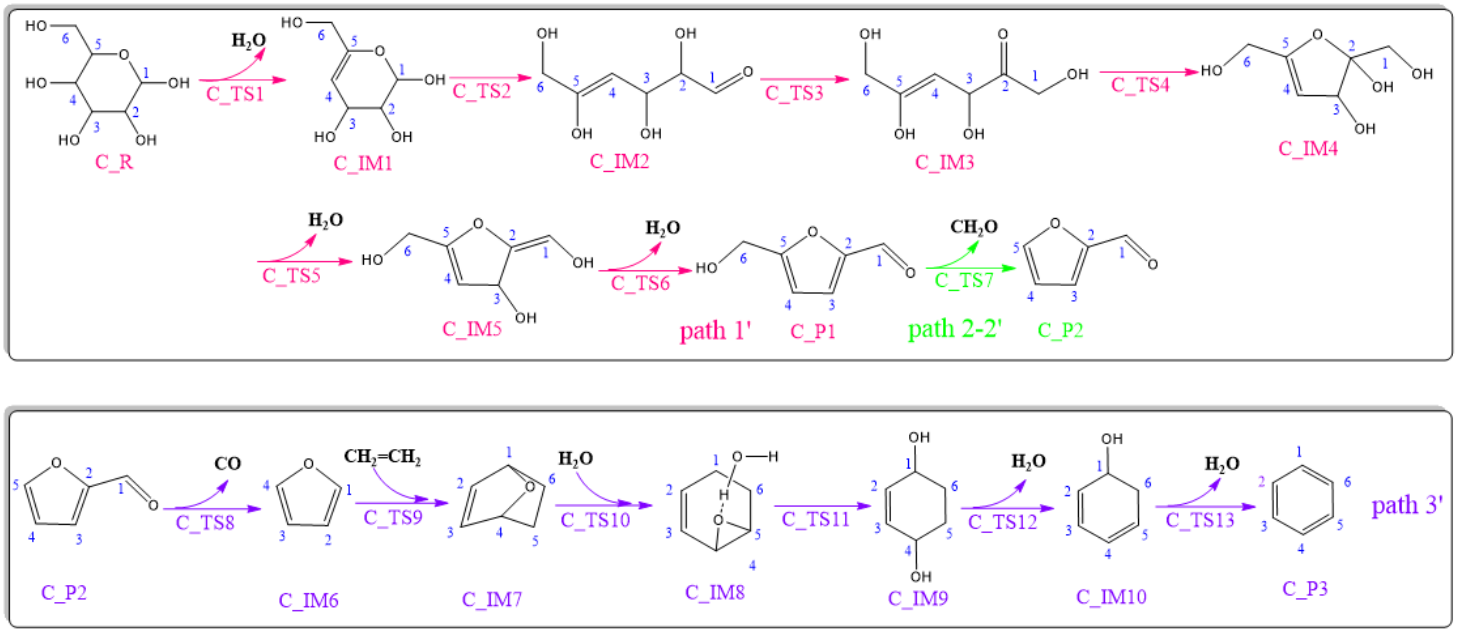

Figure 4

Catalytic pyrolysis conversion path of glucose over ZSM-5.

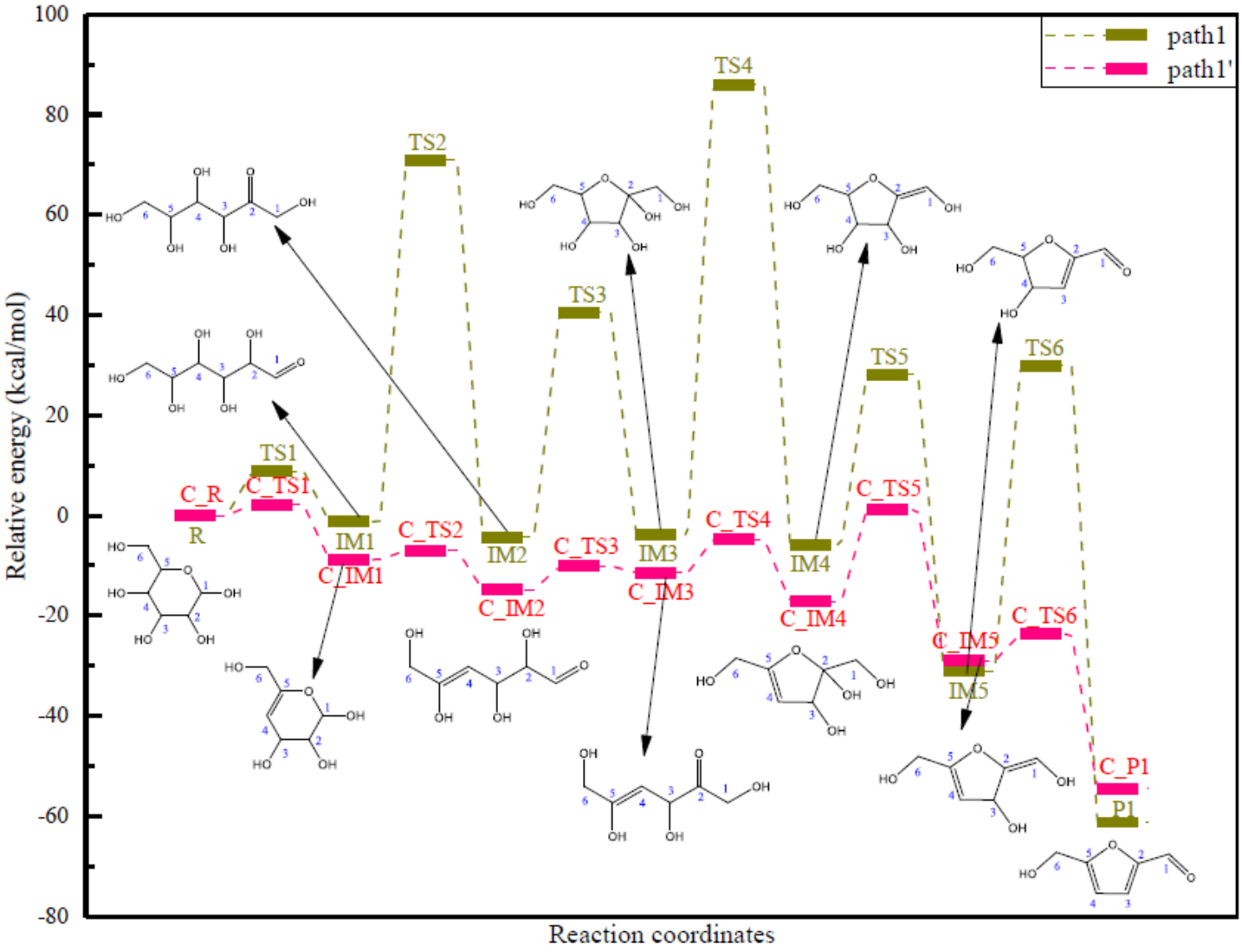

Figure 5

Catalytic and non-catalytic energy profiles of conversion from glucose to 5-hydroxymethylfurfural.

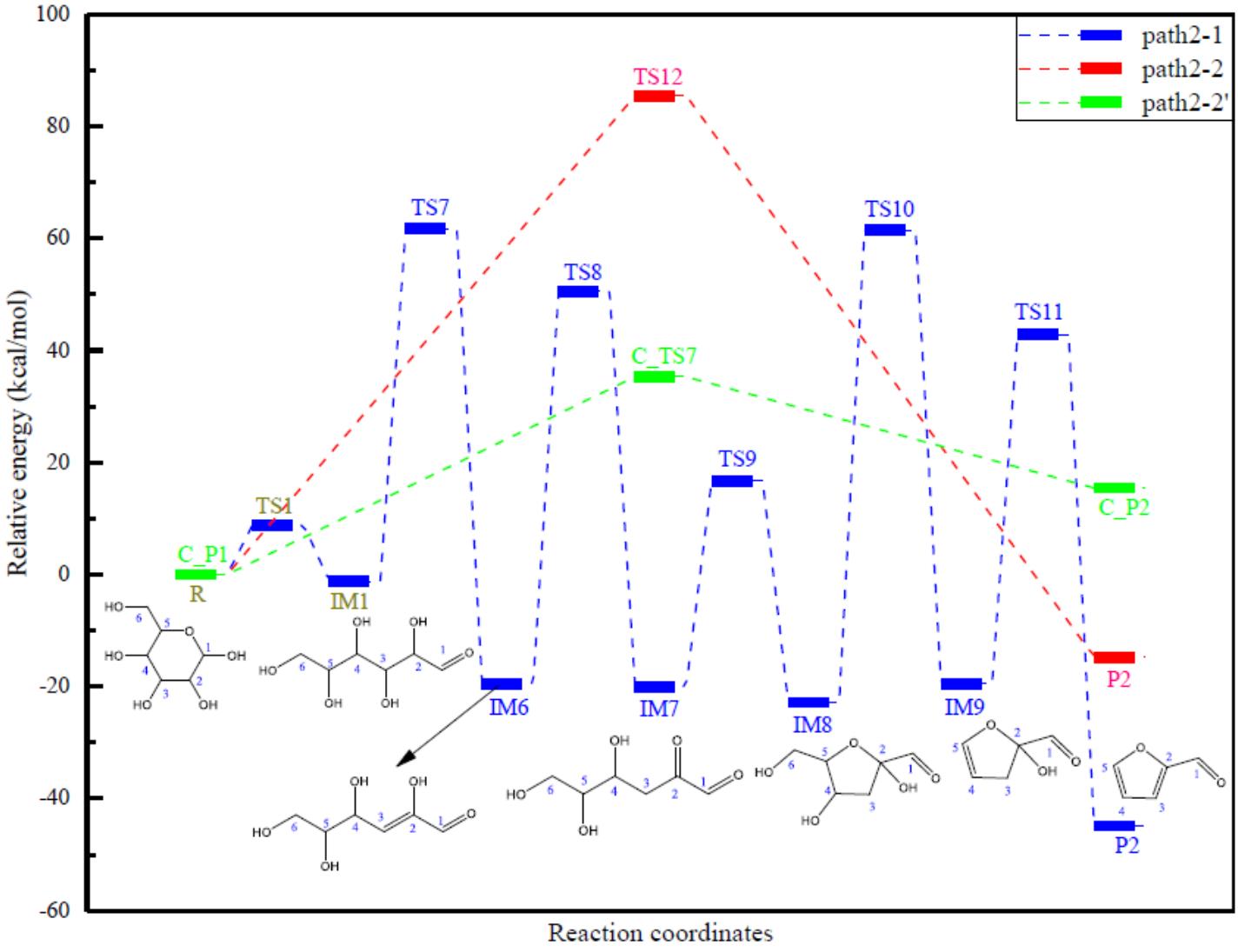

Figure 6

Catalytic and non-catalytic energy profiles of conversion from glucose to furfural.

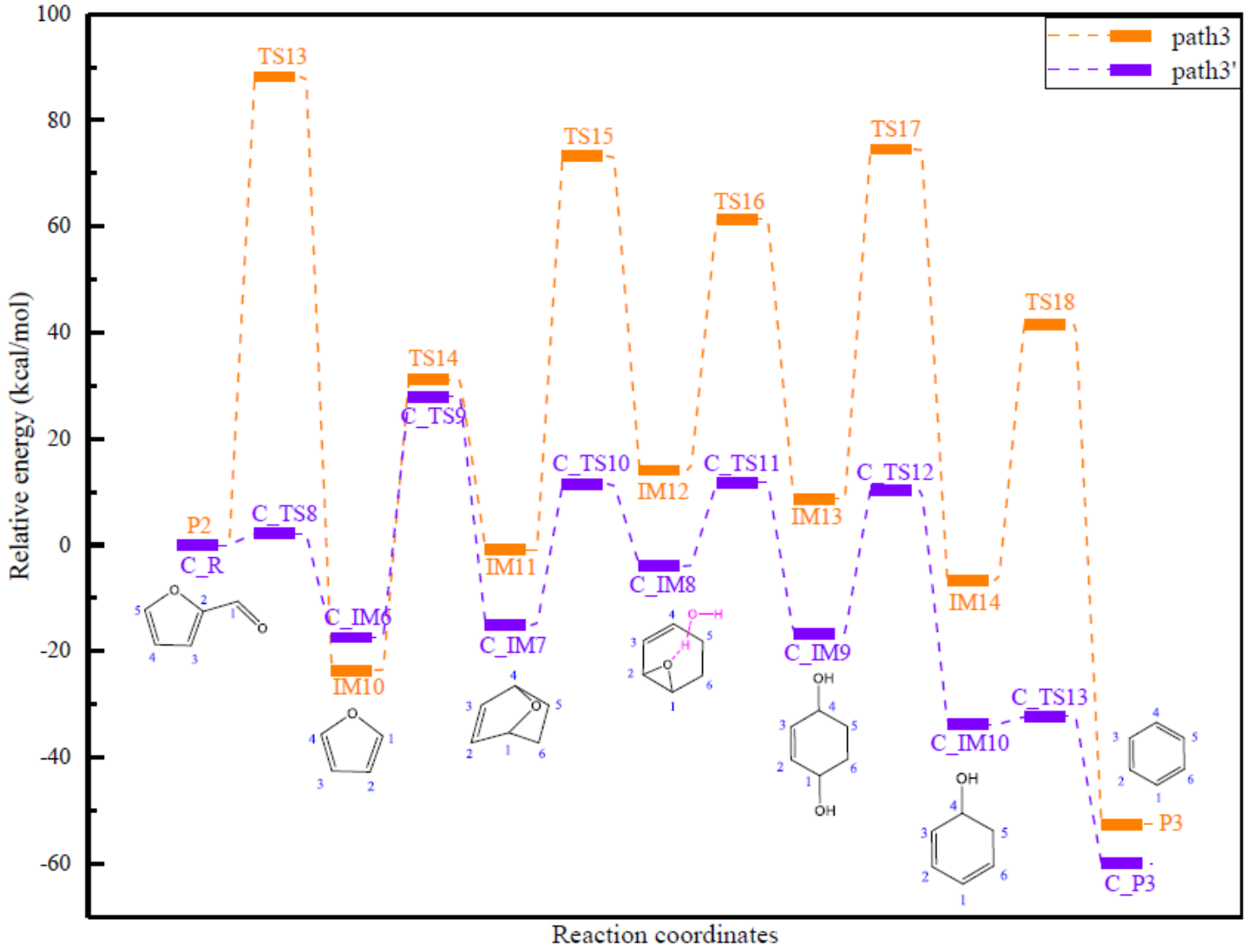

Figure 7

Catalytic and non-catalytic energy profiles of conversion from furfural to benzene.

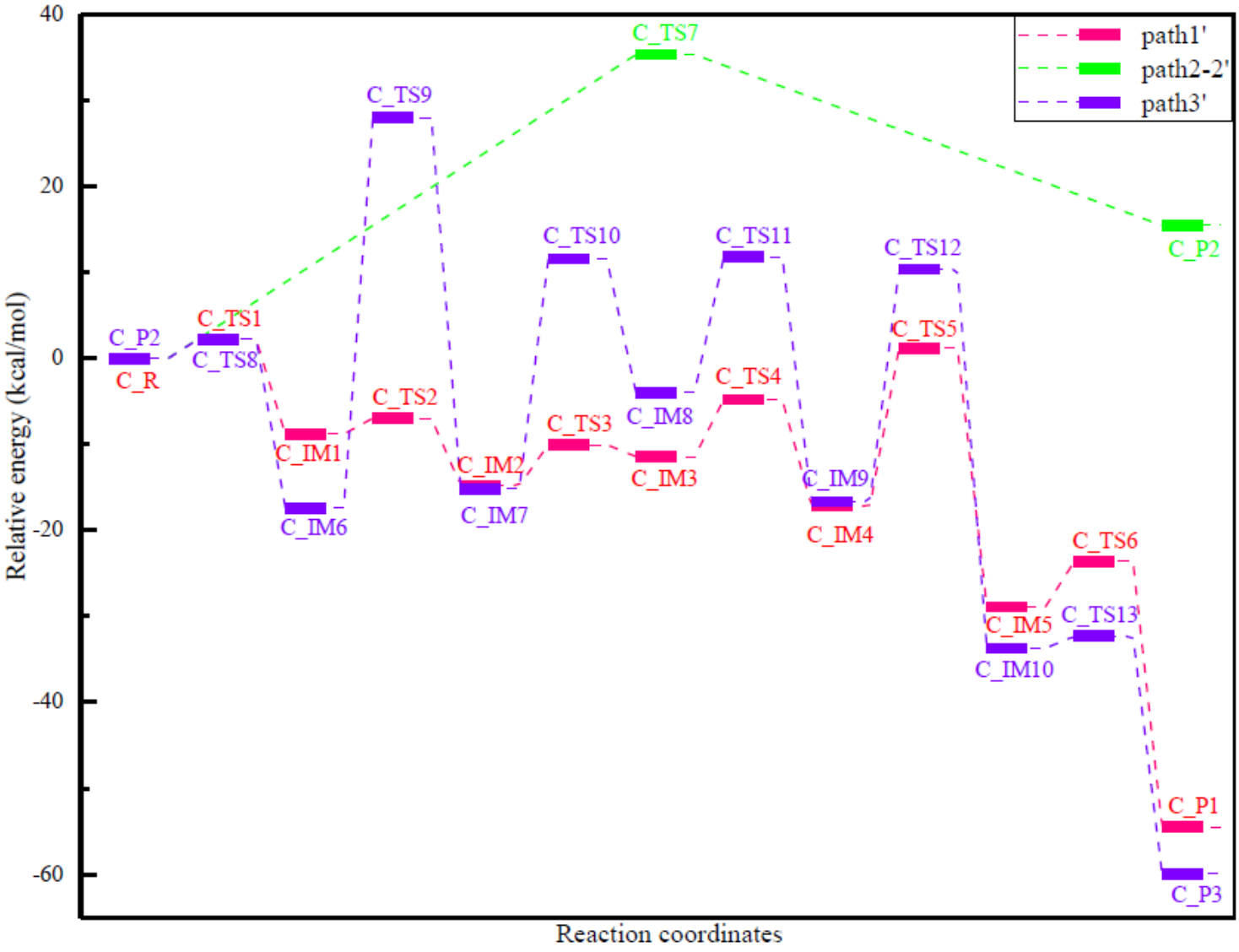

Figure 8

Energy profiles of cellulose catalytic pyrolysis.

Supplementary Files

This is a list of supplementary files associated with this preprint. Click to download.

- GraphicalAbstract.png
- Supportinformation.doc
- Tables.docx